Manganese Oxide/Carbon Nanofibers-Embedded Graphene Sheets for Capacitors

Ki-Jin Ahn[*] and Hyeonseok Yoon[*,**]

[*] Department of Polymer Engineering, Graduate School, Chonnam National University, Gwangju 500-757, South Korea.
[**] Alan G. MacDiarmid Energy Research Institute & School of Polymer Science and Engineering, Chonnam National University, Gwangju 500-757, South Korea, hyoon@chonnam.ac.kr

ABSTRACT

We report the fabrication of a ternary nanoarchitecture consisting of manganese oxide (MnO), carbon nanofibers (CNFs), and reduced graphene oxide sheets and their application to supercapacitor electrodes. MnO nanoclusters-decorated CNFs (MCNFs) with diameters of about 50 nm were prepared via single-nozzle co-electrospinning. The MCNFs were readily embedded into graphene sheets via hydrophobic interaction in aqueous solution. Importantly, this straightforward synthesis process readily affords product on a scale of tens of grams. The embedded MCNFs prevent the irreversible aggregation of graphene sheets and allow an opened microstructure inside the nanoarchitectures. The specific capacitances of the resulting nanoarchitectures were examined in an acidic electrolyte and found to be 50 to 200 F g−1 depending on the amount of reduced graphene oxide. The capacitances were higher than those of control samples (only reduced graphene oxide or MCNFs), which was probably due to the synergistic effect of the individual components. Moreover, the graphene sheets separated by the MCNFs boost the electrochemical performance of the nanoarchitecture electrodes. These electrodes exhibit enhanced specific capacitances compared with a sheet electrode fabricated of MCNF-only or RGO-only. The RGO sheet acts as a conductive channel inside the nanoarchitecture, while the intercalated MCNFs increase the efficiency of the ion and charge transfer in the nanoarchitecture. The ultrathin CNFs, which might be a promising alternative to carbon nanotubes, overcome the low electrical conductivity of the excellent pseudocapacitive component, MnO. It is expected that these structural characteristics will make the ternary nanoarchitectures promising candidates for various applications in the areas of composite science, separation/filtration, and energy conversion/storage.

Keywords: capacitors, nanofibers, graphene sheet

1 ULTRATHIN MCNFS

Ternary hybrid nanostructures consisting of CNF, MnOx , and graphene were fabricated, as illustrated in Figure 1 and Scheme 1. Poly(acrylonitrile) (PAN), poly(vinylpyrrolidone)(PVP), and manganese(II) acetate ($Mn(Ac)_2$) were first disolved in dimethylformamide (DMF), where a phase separation between the two polymers occurred. The solubility parameters of PVP, PAN, and DMF were similar with each other at 25.6, 25.3–26.1, and 24.8 $MPa^{1/2}$, respectively. Thus, PAN is theoretically miscible with pristine PVP in DMF. However, PVP has pendant lactam groups by which the polymer can coordinate with manganese ions. Specifically, the lactam group in PVP has a resonance structure with the metal ion, as illustrated in the scheme below, where the nitrogen and oxygen atoms act as a dipole.

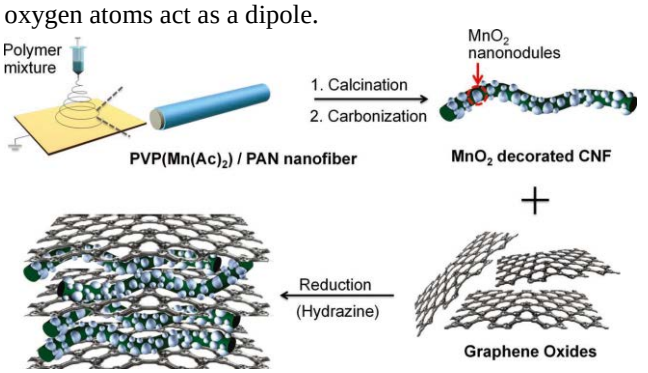

Figure 1: Schematic illustration of the fabrication of the ternary hybrid nanostructures: MCNF/RGO nanohybrids. bar is 200 nm).

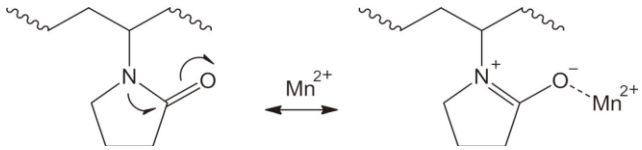

Scheme 1: The scheme shows the resonance structure of PVP with metal cations

2 RESULTS AND DISCUSSION

Such coordination of PVP with metal ions changes the miscibility of PVP with PAN, leading to a phase separation in the polymer blend. The PVP/PAN blend was observed using an optical microscope before and after the addition of manganese ions (Figure 2). The binary blend exhibited only a slight metastable behavior. However, the addition of manganese ions into the blend caused complete phase separation, where the dispersed and continuous phases were PAN and PVP, respectively. The phase-separated polymers were coelectrospun from a single nozzle. During the electrospinning, the two polymers became incompatible with DMF evaporating and the resulting phase separation

induced a microphase separated fibrous structure of manganese ion/PVP sheathed PAN nanofibers. The obtained nanofibers were subject to calcination at 400 °C for stabilization of the PAN by cyclization and concurrent conversion of the manganese ion to MnO_x. Subsequent heat treatment proceeded at 900 °C under inert atmosphere to yield MCNFs.

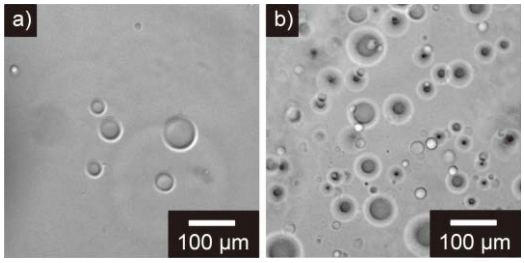

Figure 2: Optical micrographs of (a) PVP/PAN blend and (b) manganese ion-added PVP/PAN blend in DMF.

The morphology of the MCNF/RGO nanohybrids was examined using transmission electron microscopy (TEM) and the resulting MCNF images are shown in Figure 3a. The diameter of the nanofi bers was 48 ± 6 nm, which was remarkably less than that (more than 100 nm) of those normally produced by electrospinning techniques. Nanometer sized MnO_x particles with a diameter of 15 ± 5 nm were well dispersed onto the CNFs. The magnifi ed TEM image (Figure 3b) reveals lattice planes in the MnO x nanoparticles, indicating that the nanoparticles had crystalline phases. Figure 3c presents a typical crosssectional scanning electron microscopy (SEM) image of the MCNF/RGO nanohybrids (RGO 50 wt%) deposited on a silicon wafer.

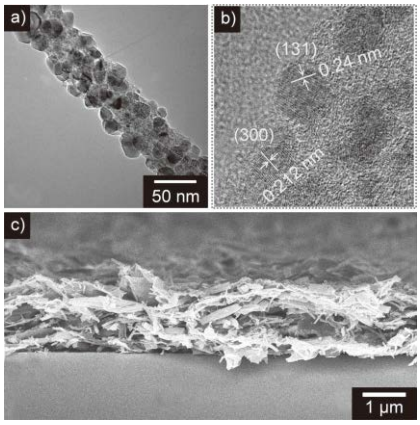

Figure 3: (a) Typical TEM image of MCNF, (b) high-resolution TEM image of MCNF (the lattice planes of γ -MnO 2 such as (131) and (300) were marked), and (c) cross-sectional SEM image of MCNF/RGO nanohybrids (RGO 50 wt%) deposited on a silicon wafer.

Figure 4a shows the full XPS spectra of four different samples over the range of 0–1200 eV. The overview spectra indicated that the nanohybrids consisted of carbon, oxygen, and manganese without any impurity. Furthermore, high-resolution XPS C 1s spectra of the samples were inspected to trace their qualitative change (Figure 4 b). For the pristine CNFs, a dominant peak centered at ca . 284.6 eV was observed, which was assigned to the graphitic sp 2 carbon atoms. Two additional peaks at 285.5 and 287.9 eV were attributed to oxygenated carbons (e.g., C-O or C=O) and nitrogenated carbons (e.g., C-N or C=N). No signifi cant change was observed in the MCNF spectrum. However, after the introduction of GO sheets, the non-graphitic carbon peaks at 285.7 and 287.9 eV grew at the expense of the graphitic sp^2 carbon peak at 283.9 eV, due to the oxygen-containing groups of GO. Importantly, the graphitic sp^2 carbon peak was recovered after the reduction of GO in the nanohybrid. Figure 4 c exhibits the high-resolution XPS Mn 2p spectrum of the nanohybrids. The main spin-orbit components (2p 3/2 and 2p 1/2) were observed at 642 and 653 eV. The splitting of the Mn 2p doublet was 11 eV, which is in accordance with that reported for MnO 2 . [35] It can therefore be concluded that the MnO x inside the nanohybrids mostly existed in the form of MnO 2 . The nanohybrids were further characterized by X-ray diffraction (XRD) analysis (see Supporting Information). MnO 2 peaks were observed in the spectrum of MCNFs. The peak intensity became weakened after hybridization with RGO due to the peak superposition. Relatively intense peaks at 2 θ = 28, 37, 41, and 65 ° could be traced in the XRD spectrum, which were assigned to (310), (131), (300), and (421) planes of γ-MnO_2.

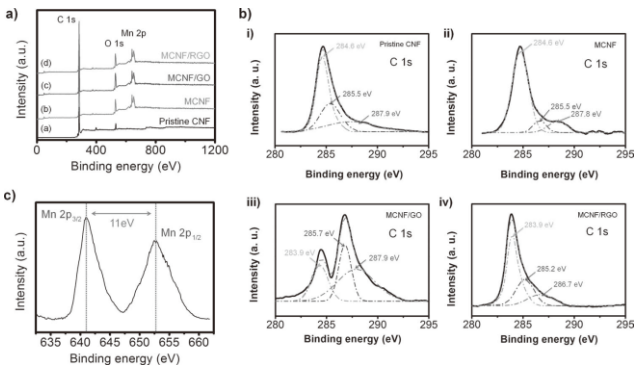

Figure 4: (a) Full XPS spectra and (b) high-resolution XPS C 1s spectra of MCNF/RGO nanohybrids and control samples (pristine CNF, MCNF, and MCNF/GO). (c) High-resolution Mn 2p spectrum of MCNF/RGO nanohybrids.

To assess the potential of the MCNF/RGO nanohybrids as electrode materials for electrochemical capacitors, fi rst, their electrochemical properties were investigated using cyclic voltammetry (CV) in three-electrode cells (Figure 5). The nanohybrids with different MCNF/RGO ratios were tested, together with their individual components (MCNFs and RGO) for comparison under the same experimental condition.The MCNF/GO nanohybrids were also employed as a control to demonstrate the role of RGO in the nanohybrids.

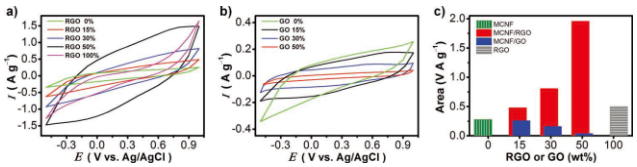

Figure 5: (a) Full XPS spectra and (b) high-resolution XPS C 1s spectra of MCNF/RGO nanohybrids and control samples (pristine CNF, MCNF, and MCNF/GO). (c) High-resolution Mn 2p spectrum of MCNF/RGO nanohybrids.

Galvanostatic charge-discharge measurements were obtained from the samples to obtain more detailed information on their specifi c capacitance (Figure 6a and c), and the specific capacitances were determined from the discharging curves (Figure 6 b and d). The potential range was chosen by taking into account the CV curves. The current density was fi xed at 0.2 A g − 1 for direct performance comparison between the individual samples. All the curves exhibited good reversibility during the charge/discharge process at the corresponding potential range.

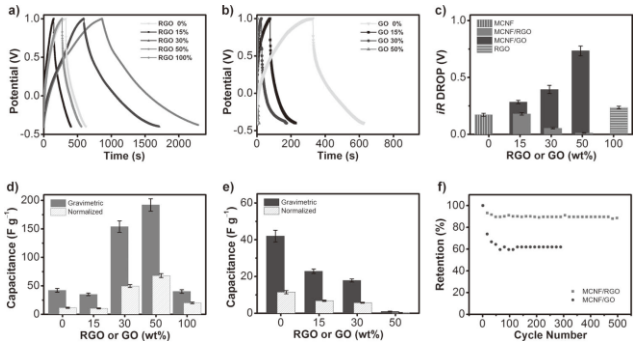

Figure 6: Galvanostatic charge/discharge curves (a) MCNF/RGO nanohybrids and (b) MCNF/GO measured with a current density of 0.2 A g − 1 . (c) iR drop values obtained from the charge/discharge curves. Capacitance values for (d) MCNF/RGO nanohybrids and (e) MCNF/GO calculated from the charge/discharge curves. (f) Long-term cycling performances of MCNF/RGO (50 wt%) nanohybrids and MCNF/GO.

Electrochemical impedance spectroscopy (EIS) measurements were carried out to further understand the electrochemical and structural characteristics of the electrode material (Figure7). All the Nyquist plots exhibited a semicircle over the high frequency range, followed by a linear part in the low frequency section. The intercept for the real component at the beginning of the semicircle indicated the combined series resistance of the electrolyte, electrode, current collectors, and the electrode/current collector contact resistance. The resistances of the electrolyte and current collectors were equivalent for all samples. The intercepts of the nanohybrid electrodes ranged from 0.25–0.29 Ω cm 2 , which were entirely lower than the value of MCNF (0.30 cm 2) or RGO (0.33 cm 2) electrodes. Such data are commensurate with the results obtained from the iR drop. The electrodes containing MnO_x component presented a slight inclination at the initial stage of the linear part, which was attributed to the presence of pseudocapacitance.

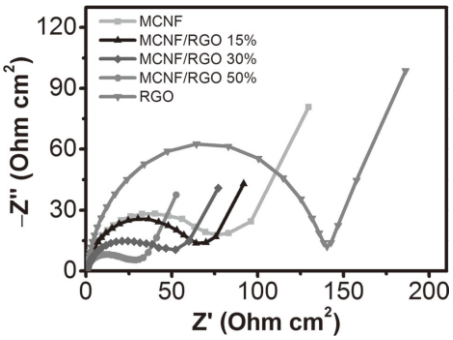

Figure 7: (a) Full XPS spectra and (b) high-resolution XPS C 1s spectra of MCNF/RGO nanohybrids and control samples (pristine CNF, MCNF, and MCNF/GO). (c) High-resolution Mn 2p spectrum of MCNF/RGO nanohybrids.

REFERENCES

[1] J. S. Lee, O. S. Kwon, S. J. Park, E. Y. Park, S. A. You, H. Yoon, J. Jang, “Fabrication of ultrafine metal-oxide-decorated carbon nanofibers for DMMP sensor application”, ACS Nano, 2011, 5 (10), 7992–8001

[2] Y. Huang, J. Liang, Y. Chen, “An Overview of the Applications of Graphene-Based Materials in Supercapacitors”, Small, 2012, 8, 1805 – 1834

[3] B. Luo, S. Liu, L. Zhi, “Chemical Approaches toward Graphene-Based Nanomaterials and their Applications in Energy-Related Areas”, Small, 2012, 8, 630 – 646

[4] O. S. Kwon, S. J. Park, H. -W. Park, T. Kim, M. Kang, J. Jang, H. Yoon, Kinetically Controlled Formation of Multidimensional Poly(3,4-ethylenedioxythiophene) Nanostructures in Vapor-Deposition Polymerization, Chem. Master, 2012, 22, 4088-4092.